Structure of PMMA/EGDMA Star-Branched Microgels

Peter Lang and Walther Burchard*

Institute of Macromolecular Chemistry, University of Freiburg, Stephan Meier Strasse 31, Freiburg i. Br., FRG

Michael S. Wolfe,* Harry J. Spinelli, and Loretta Page

E. I. du Pont de Nemours and Company, Experimental Station, Wilmington, Delaware 19880-0356

Received August 2, 1990; Revised Manuscript Received September 17, 1990

ABSTRACT: Star-branched microgels (SBM's), prepared by the reaction of living poly(methyl methacrylate) chains with ethylene glycol dimethacrylate, were characterized by static and dynamic light scattering, viscometry, and size-exclusion chromatography with a low-angle laser light scattering detector. The average number of arms per microgel, the arm length, the size of the microgel, the molecular weight distribution, and the frequency distribution of arms per SBM were determined. The influence of branching on the shrinking factors of the SBM's relative to linear polymers was found to deviate, as expected, toward hard-sphere behavior. After correction for polydispersity, qualitative agreement with regular star polymers was found for the interdependence of the radius of gyration and intrinsic viscosity shrinking parameters. Unexpectedly, it was found that the ratio of the hydrodynamic volumes of SBM's to linear polymers at the same molecular weight is dependent on the number of arms but independent of the arm molecular weight.

Introduction

It is well-known that branched macromolecules have dimensions that differ from those of linear chains of the same chemical composition and molecular weight.[1] For regularly branched materials, e.g., star-branched macromolecules, the effect of branching becomes noticeable by (i) a decrease of the mean-square radius of gyration,[1] $\langle S^2 \rangle$, (ii) a decrease of the intrinsic viscosity,[2] $[\eta]$, (iii) an increase of the translational diffusion coefficient,[3] D_z, and (iv) a decrease in the second virial coefficient,[4] A_2.

More complicated are the effects with *randomly* branched materials. The complexity arises from the extraordinary width in the molecular weight distribution,[5] which easily can reach values of $M_w/M_n \cong 100$, masking the branching effects.[6-8] The properties of macromolecules are, for practical reasons, mostly compared at the same *weight-average* molecular weights of the branched and linear chains. However, the dimensions, e.g., $\langle S^2 \rangle$ and $1/R_h$ (where R_h is the hydrodynamic radius) are *z-averages*, which weight more strongly the larger molecules. Similar broad molecular weight distributions are, however, in most cases not available for the corresponding linear chains that are taken as the reference state. The different weighting of the dimensions and of the molecular weights causes a compensation of the branching effect such that the *z*-average dimensions of the branched samples can become larger than those of the linear chains. The intrinsic viscosity, $[\eta]$, and the second virial coefficient, A_2, are not so strongly affected by polydispersity for reasons that will be discussed later in this paper.

The samples of the present study were expected to show properties in between those of the regularly and the randomly branched classes. This expectation results from the procedure of preparation that in brief is as follows. In a first step linear PMMA prepolymers are synthesized via group-transfer polymerization (GTP).[9] Following the addition of ethylene glycol dimethacrylate (EGDMA), the still active end groups of the PMMA chains initiate the polymerization of EGDMA, which, via its two double bonds, leads immediately to cross-linking. However, no macrogelation occurs, evidently because of the long-tailed initiators (the PMMA prepolymers). Instead of a macrogel, soluble microgels are obtained with many dangling PMMA chains, and the whole structure resembles now a star-branched macromolecules but with a cross-linked microgel as its center.[10] We will call the resulting polymers star-branched microgels (SBM).

This molecular architecture raises a number of questions: (1) How many chains are attached to the microgel, and does the number depend on the length of the prepolymer chain? (2) How large is the microgel? (3) What is the molecular weight distribution? (4) How are the shrinking factors affected by this architecture?

Molecular weight distributions are nowadays determined mainly by gel permeation chromatography (GPC), sometimes called size-exclusion chromatography (SEC). The common understanding of the fractionation process is that the different molecular sizes are separated according to the hydrodynamic volume rather than according to their molecular weight.[11] Therefore, for branched polymers, a simple GPC experiment using linear polymers for molecular weight calibration will give an incorrect molecular weight distribution since the hydrodynamic volume depends in a complex way on the branching density as well as the molecular weight.

A correct molecular weight distribution may be obtained, however, if the common GPC is combined with an on-line molecular weight determination by low-angle laser light scattering (LALLS). This technique was applied to PMMA star-branched microgels and gave a surprising result, which has been reported previously in brief[12] and which will be discussed in greater detail below.

Our study of star-branched microgels is divided into two parts. In the present contribution we describe the LALLS technique and report the results of polymer characterization in dilute solution by static and dynamic light scattering and by viscometry. The data are discussed in terms of branching theories. In a second part we will report findings with these samples in the semidilute and moderately concentrated solutions. The results are compared with other architectures and tentatively interpreted by the recent renormalization group theory.

0024-9297/91/2224-1306$02.50/0

Table I
Star-Branched Microgel Samples: Polymerization Conditions and Arm Molecular Weights

sample	initial charge: THF, g	initial charge: 1 M TBCB, mL	initiator: TMSMMP, g	feed I: THF, g	feed I: 1 M TBCB, mL	feed II, g of MMA	feed III, g of EGDMA	$(M_w)_{arm}$
S10	90	50	0.90	5.62	50	51	6.0	1.1×10^4
S20	200	50	0.90	3.6	50	101	6.0	2.7×10^4
S21a	200	170	2.30	5.62	170	101	15.7	9.3×10^3
S21b	200	80	1.40	5.62	80	101	10.8	1.5×10^4
S21c	200	50	0.90	5.62	50	101	6.1	2.8×10^4

Experimental Section

While all the star-branched microgels were prepared in one of our laboratories (Du Pont), the solution properties were studied independently in both laboratories (Freiburg and Du Pont). For the SBM samples to be discussed below, samples S10, S10f, S20, and S20f were studied at Freiburg while samples S21a, S21b, and S21c were studied at Du Pont.

Samples. PMMA star-branched microgels having different arm lengths were prepared by first synthesizing living PMMA precursor chains by group-transfer polymerization (GTP) followed by adding ethylene glycol dimethacrylate (EGDMA) to the reaction medium. The EGDMA to PMMA precursor chain mole ratio was approximately 6:1. The PMMA chains are then coupled via the cross-linking reaction of EGDMA. Finally, a densely cross-linked microgel is obtained with a number of PMMA dangling arms of high uniformity.

The coupling reaction was not fully efficient, and a small fraction of unattached linear chains was obtained in addition to the SBM. The linear fraction could easily be separated by precipitation fraction from THF solutions with methanol, where the SBM precipitated while the linear moiety remained in solution. For the S10 sample, a larger amount of the linear fraction (L10) was recovered by solvent evaporation and complete precipitation with methanol. The fractionated samples were redissolved in dioxane and freeze-dried. The obtained mass was sufficient for a molecular weight determination by static light scattering as well as dynamic light scattering studies. For sample S20, the molecular weight of the arm was determined only by GPC using a calibration curve for linear PMMA in THF, obtained with samples described below. The star microgels, free of linear chain, are denoted as S10f and S20f. Samples S21a, S21b, and S21c had been precipitated from THF with hexane. This resulted in a small portion of free arm remaining (~5–10%) in the samples.

Four other linear PMMA samples in the range of M_w = 64 500–1.47×10^6 were products of the Röhm Co., Darmstadt, and were prepared again by GTP. Finally, one sample of M_w = 20 000 was prepared at Freiburg using a GTP prescription by Müller.[13]

Star-Branched Microgel Syntheses. A 1-L flask was equipped with a mechanical stirrer, thermometer, nitrogen gas inlet, drying tube outlet, and addition funnels. The temperature was maintained at room temperature (~25 °C). The solvent, tetrahydrofuran (THF), and catalyst, tetrabutylammonium *m*-chlorobenzoate (TBACB), were charged to the flask. The initiator, 1-(trimethylsiloxy)-1-methoxy-2-methylpropene (TMSMMP), was injected. Feed I, containing THF and TBACB, was then started and added over a 120-min period. Feed II consisting of the monomer methyl methacrylate (MMA) was started and added over a 30-min period. Feed III, consisting of the cross-linker, EGDMA, was started 35 min after the end of feed II and added over a 10-min period. At 200 min the reaction was quenched with methanol. Table I lists the reagent quantities for the different additions.

To determine the arm molecular weights, parallel reactions were run through the second feed and quenched prior to the addition of the cross-linker. The resulting GPC curves were taken as representative of the PMMA arms for the SBM's. The weight-average molecular weights for the arms determined in this manner are listed in Table I.

NMR. The EGDMA/MMA composition was determined by NMR with a Bruker 250-MHz high-resolution spectrometer comparing the peak areas resulting from the $-OCH_2$ and $-OCH_3$ protons.

Viscometry. A Schott SAV automatic viscometer (Schott, Mainz, FRG) was used for determination of the viscosities in THF. The dilution of a stock solution was made automatically, and the intrinsic viscosity was obtained after extrapolation to zero concentration in the usual manner. For SBM samples S21a, S21b, and S21c, viscosities were determined with Cannon–Fenske capillary viscometers.

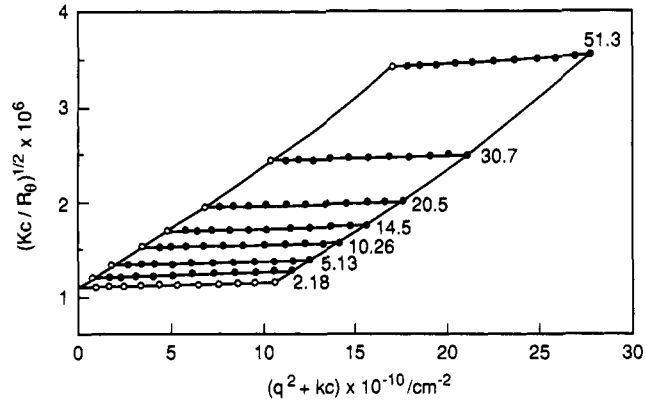

Figure 1. Berry plot for sample S10f in THF at 20 °C. The numbers in the plot denote the concentrations in milligrams per milliliter.

Light Scattering. Static (SLS) and dynamic (DLS) light scattering measurements were performed simultaneously in THF at 20 °C by using the ALV 3000 correlation spectrometer system (ALV Langen, Hessen, FRG). The setup has been described in detail previously.[14] An argon ion laser Ar 165 from Spectra Physics was used as light source with a wavelength of λ_0 = 488 nm. The scattering measurements were carried out in an angle range from 20 to 150° in steps of 10°. For samples S21a, S21b, and S21c dynamic light scattering measurements were performed at λ_0 = 514.5 nm over a similar angular range and temperature using a Brookhaven Instruments BI-200SM goniometer and BI-2030AT correlator with a Lexel 75-3 argon ion laser.

All solutions were first clarified by filtering them through nucleopore filters of 0.2-μm pore size. The low molecular weight samples were in addition treated by ultracentrifugation using the floating technique.[15] Here the LS cells (0.8-cm diameter and 7-cm length) are suspended in an aqueous CsCl solution of the required density and spun at 10 000 rpm in a Beckman L5-50B ultracentrifuge.

The data of the LS measurements were evaluated from static and dynamic Zimm plots where Kc/R_θ or Γ/q_2 is plotted against $q^2 + Kc$. Here K is the usual optical contrast factor, which is essentially defined by the refractive index increment dn/dc; c is the concentration, R_θ is the scattering intensity (Rayleigh ratio), Γ is the first cumulant of the time correlation function in dynamic LS, and $q = (4\pi/\lambda) \sin \theta/2$ is the value of the scattering vector that is related to the scattering angle θ and the wavelength of the light in the medium $\lambda = \lambda_0/n_0$ with n_0 the refractive index of the solvent. The refractive index increment dn/dc = 0.0883 of PMMA in THF at λ_0 = 488 nm was obtained by interpolation of literature values[16] at wavelengths of 436 and 546 nm. The star microgels were also measured by LALLS with a laser of the wavelength of λ_0 = 633 nm, and the corresponding refractive index increment dn/dc = 0.0850 was measured with a Brice–Phoenix differential refractometer.

GPC-LALLS. For samples S21a, S21b, and S21c, measurements were performed at LDC/Milton Roy Co. The column bank consisted of 50-, 10^2-, 10^3-, and 10^4-nm Ultrastyragels in series. The low-angle (6°) light scattering was detected with LDC/Milton Roy KMX-6 low-angle laser light scattering pho-

Table II
Solution Properties of Star-Branched (S Series) and Linear (L Series) PMMA in THF at 20 °C

sample	$M_w \times 10^{-5}$, g/mol	$A_2 \times 10^5$, mol·mL·g^{-2}	R_g, nm	$D_z \times 10^7$, cm^2/s	R_h, nm	$[\eta]$, mL/g	ρ
S10	8.55	3.86	14.6	3.06	13.47	13.5	1.08
S20	5.26	13.0	14.8	3.06	13.47	30.0	1.10
S10f	9.03	4.82	14.1	3.18	13.18	19.3	1.07
S20f	4.54	17.0	14.8	3.04	13.04	26.2	1.13
S21a	9.97	5.19		2.77	14.1	13.8	
S21b	6.64	5.48		3.20	12.2	16.7	
S21c	5.74	7.16		2.67	14.6	25.0	
PL1	0.20	83.2		14.0	2.95		
L10	0.25	72.4		13.6	3.03		
L4	0.645	58.0	9.5	7.6	5.43	24.5	1.74
L3	1.66	47.3	16.5	4.3	9.59	48.5	1.72
L2	7.27	43.2	36.8	2.0	20.62	125.9	1.76
L1	14.7	32.0	54.3	1.35	30.54	199.3	1.78

tometer equipped with a flow-through cell. Conversion of the light scattering intensity to molecular weight was performed by standard procedures. The refractive index was detected with a LDC/Milton Roy Refractomonitor III to provide the relative polymer concentration as a function of elution volume. A flow rate of 1.00 mL/min was maintained for the THF mobile phase. The analogue data were electronically digitized and processed with standard LDC/Milton Roy software.

For samples S10, S10f, S20, and S20f, measurements were performed at Freiburg using similar instrumentation and procedures. The chromatograms were run with an analogue recorder and subsequently digitized by using a HIPAD digitizer (Housten Instruments).

Theoretical Basis of the LALLS

In the LALLS technique, the same basic equations are used as in common LS measurements.

$$\frac{Kc}{R_\theta} = \frac{1}{M_w P(\theta)} + 2A_2 c \tag{1}$$

Here, M_w is the weight-average molecular weight of the polymer, A_2 the second virial coefficient, and c the mass concentration. The apparent particle scattering factor, $P(\theta)$, gives information about the size and the shape of the particle and describes the angular dependence of the intensity of the scattered light.

For small values of $u^2 = q^2\langle S^2\rangle$ the particle scattering factor can be expressed in a power series

$$P(\theta) = 1 - (1/3)u^2 + \ldots \tag{2}$$

and if $u^2 \ll 1$, one has $P(\theta) = 1$. For flexible chains with $R_g < 100$ nm, the condition $u^2 \ll 1$ at $\theta = 6°$ is fulfilled (at $q = 2 \times 10^{-3}$ nm^{-1} and $R_g = 100$ nm, one has $u^2/3 < 1.3 \times 10^{-2}$). The virial coefficient needed in eq 1 can be determined by light scattering from the nonfractionated sample. This value can be used as a good approximation for the fractions since A_2 is only a weakly decreasing function of M_w.

Results

Molecular Parameters. The molecular parameters were obtained from static and dynamic LS in dilute solutions. In this concentration range the interaction between the polymer molecules is small such that the parameters of individual macromolecules are obtained after extrapolation of the experimental data to zero concentration. Zimm plots of the SBM's exhibit significant nonlinear concentration dependence of the scattering intensity, indicating a nonnegligible third virial coefficient. For this reason, a reliable extrapolation of the apparent molecular weights to zero concentration is not possible. Instead, Berry plots[19] were made by plotting

$$(Kc/R_{\theta=0})^{1/2} = (1/M_w)^{1/2}(1 + A_2 M_w c) \tag{3}$$

against c. Figure 1 shows a Berry plot for the star-branched microgel S10f. This plot allows a reliable determination of molecular weight M_w and the second virial coefficient A_2. The intercept in this plot gives $(1/M_w)^{1/2}$ and the slope divided by the intercept $A_2 M_w$.

The hydrodynamic radii, R_h, of the polymers were determined by dynamic LS, which was measured simultaneously to the static LS experiments. Dynamic LS allows the determination of the translational diffusion coefficients D_z from the initial slope of the field time correlation function[20] (TCF), ln $(g_I(t))$, as a function of time, t. This initial part of the TCF can be approximated by a cumulant expansion.[21,22] In the limit of zero scattering angle, the first cumulant, Γ, is related to the diffusion coefficient[20]

$$\Gamma = D_c q^2 \tag{4}$$

In most cases, the diffusion coefficient D_c at concentration c depends linearly on c and gives at $c = 0$ the z-average translational diffusion coefficient, D_z. The hydrodynamic radius may now be defined by applying the Stokes–Einstein equation

$$D_z = kT(6\pi\eta_0 R_h) \tag{5}$$

where k is the Boltzmann constant and η_0 the solvent viscosity.

Table II presents the data for M_w, $R_g = (\langle S^2\rangle_z)^{1/2}$, A_2, D_z, and R_h in tetrahydrofuran (THF) of the branched samples and a number of linear PMMA polymers.

Molecular Weight Distribution. The determination of molecular weight distributions was carried out by GPC–LALLS. Figure 2 shows typical chromatograms of the star-branched microgels. The full lines represent the light scattering intensity in arbitrary units whereas the dashed lines represent the concentration that was recorded by a refractive index (RI) detector. Curve a refers to the star microgel S21a. Although the RI detector shows the presence of nonattached arms, for the determination of the SBM molecular weight distributions, the nonattached arm contribution to the chromatograms was neglected. Indeed, with the light scattering detector, curve a demonstrates that the contribution of the nonattached arms is negligible. Curves b and c refer to the star-branched microgel prior to (S10) and after (S10f) fractionation, respectively. The RI detector chromatogram shows the presence of only one peak after fractionation, indicating complete removal of the nonattached arms. The presence of a second peak for the light scattering chromatogram in curve b is not understood since this peak does not

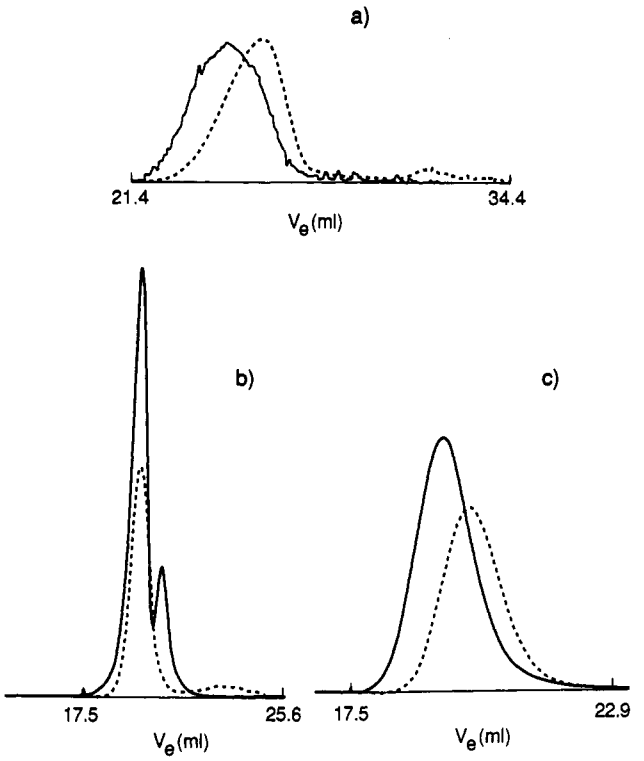

Figure 2. GPC elution curves; full and dashed lines represent elution curves using a low-angle laser light scattering detector and a refractive index detecter, respectively. Samples: (a) S21a (unfractionated); (b) S10 (unfractionated); (c) S10f.

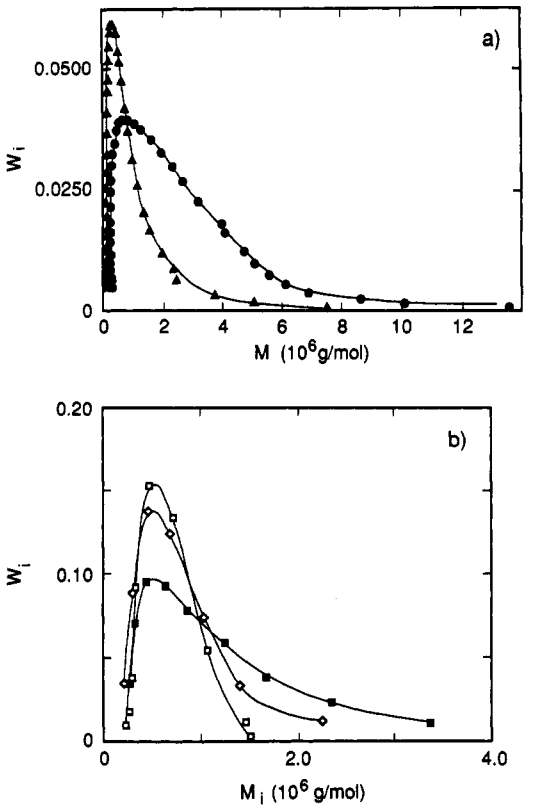

Figure 3. Relative mass fraction as function of molecular weight: (a) samples S10f (●) and S20f (▲); (b) samples S21a (■), S21b (◊), and S21c (□).

correspond to the nonattached arm peak from the RI chromatogram. Finally, the peak positions for the RI vs light scattering chromatograms shift with respect to each other prior to and following fractionation. This may be a result of an inadvertent change in the molecular weight distribution during the fractionation process.

The Rayleigh ratio, R_θ, is defined as the ratio of the scattered to the primary beam intensities; both are measured by the LALLS instrument. Thus, for every point of the curve, a molecular weight can be calculated and the molecular weight averages M_w and M_n of the sample could be obtained by using the common statistical definitions.

Both LALLS (V_e) and RI (V_e) are measured as a function of the elution volume, V_e. Elimination of V_e leads to the weight fraction distribution of the investigated sample. Figure 3a shows the distributions of the star-branched microgels S10f and S20f, and Figure 3b is a similar plot for S21a, S21b, and S21c. One notices that the width of the distribution is not particularly large in total, but the curves have a long high molecular weight tail. With increasing arm molecular weight as listed in Table I, the peak in the distribution shifts to lower molecular weight and the distribution narrows.

To demonstrate the efficiency fo the GPC–LALLS technique, the molecular weights of the star-branched microgels are listed in Table III as they were determined: (i) by static LS, (ii) by GPC alone, using a calibration curve for linear PMMA, and (iii) by GPC–LALLS. It also contains the polydispersity indices M_w/M_n as were found by the GPC–LALLS method. Application of a simple GPC calibration curve that was obtained with linear PMMA samples gives evidently a wrong result. Not only are the molecular weights much too low compared with direct LS measurements but also the trend is reversed; i.e., the low molecular weight sample is found by simple GPC to have a higher molecular weight. Application of the GPC–LALLS combination, on the other hand, leads to a very satisfactory agreement with direct M_w measurements by static LS (5–10% error).

Table III
Weight-Average Molecular Weights for Star-Branched Microgels

sample	M_w, 10^5 g/mol by LS	by GPC[a]	by GPC–LALLS	$M_w{}^b/M_n$
S10f	9.03	1.9	8.21	1.82
S20f	4.54	2.8	4.66	1.72
S21a	9.97	1.5	8.68	1.66
S21b	6.64	1.5	6.73	1.37
S21c	5.74	1.7	5.76	1.25

[a] Using linear PMMA calibration. [b] Determined by GPC–LALLS.

Number of Arms. It is known that linear PMMA chains, synthesized by GTP, have a low polydispersity.[13] Thus, the relatively high polydispersities of the SBM's are not caused by differences in the arm length of the stars but are a result of a variation in the number of arms per microgel, i.e., the polydispersity of the microgel.

Since the total molecular weights of the SBM were measured by static LS and the individual arm molecular weights are known from GPC experiments, the weight-average number of arms per microgel, f_w, can be estimated by dividing the total molecular weight by that of one arm. Values of f_w calculated in this manner are in the range of 10–100 arms as listed in Table IV. This estimate neglects the contribution of the EGDMA to the molecular size of the SBM. NMR spectrometry revealed that the weight fraction of EGDMA in the polymer is small, in the range of 3–5%. The actual values of f_w will be approximately 5% smaller than the values listed in Table IV. Therefore, this approximation only results in a small error in f_w and does not invalidate the observed trend of a decreasing f_w with increasing arm molecular weight.

The same approximation (i.e., neglecting the mass of the microgel core) was applied to very narrow fractions of

Table IV
Shrinking Factors for the Star-Branched Microgels in THF

sample	f_w	g	g_w[a]	g_{reg}[b]	h	h_{reg}[c]	g_{A_2}	ψ^*_b[d]	$g_{A_2}/g^{2/3}$	g'
S10f	80	0.141	0.095	0.037	0.551	0.265	0.119	1.65	2.25	0.133
S20f	17	0.303	0.209	0.170	0.839	0.541	0.385	1.37	2.31	0.260
S21a	93				0.868	0.247	0.127			0.098
S21b	45				0.862	0.349	0.127			0.140
S21c	21				1.12	0.494	0.161			0.232

[a] $g_w = \langle S^2\rangle_{w,b}/\langle S^2\rangle_{lin}$, where the polydispersity of Table III was used and the relationship $\langle S^2\rangle_z/\langle S^2\rangle_w = (z+1+2\nu)/(z+1)$ with $1/z = M_w/M_n - 1$. [b] $g_{reg} = (3f-2)/f^2$ for regular star-branched polymers. [c] $h_{reg} = f^{1/2}/[(2-f)+2^{1/2}(f-1)]$ for regular star-branched polymers. [d] $R_g = (\langle S^2\rangle_w)^{1/2}$ was used in eq 22.

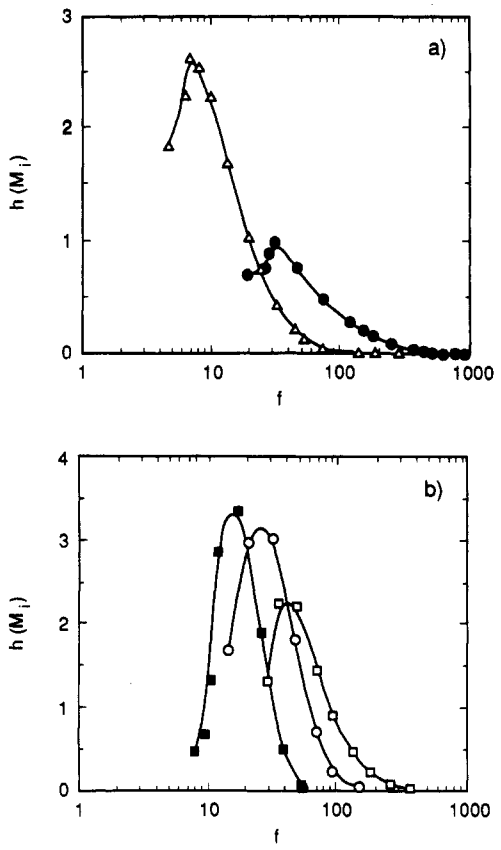

Figure 4. Relative frequency distributions for the number of arms: (a) samples S10f (●) and S20f (△); (b) samples S21a (□), S21b (○), and S21c (■).

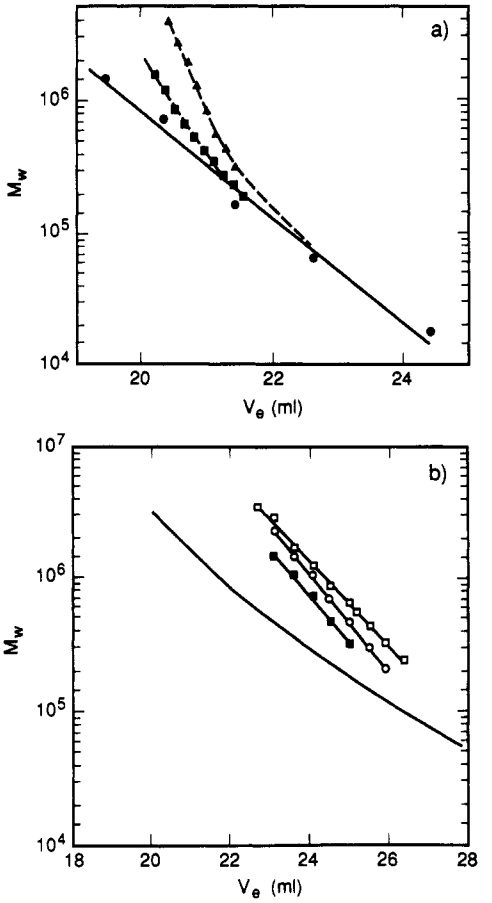

Figure 5. Relationship between molecular weight and elution volume for (a) linear PMMA chains (●) and the star-branched microgels S10f (▲) and S20f (■); (b) star-branched microgels S21a (□), S21b (○), and S21c (■). Solid curve represents linear PMMA molecular weight calibration.

the whole distribution, allowing the determination of the number distribution of the star-branched microgels expressed in terms of the number of arms per microgel. These distributions are plotted for the different SBM's in Figure 4. It is noteworthy that with increasing arm molecular weight the SBM's exhibit a lower degree of branching.

It is of interest to compare the GPC calibration curves of the SBM's with that obtained from a series of linear PMMA chains. Figure 5 shows that the elution volume for samples of the same molecular weight increases with branching. This fact will be analyzed in more detail in the following section together with the other branching properties. The linear polymer GPC calibration curves shown in parts a and b of Figure 5 as determined at Freiburg and Du Pont, respectively, are different. This is because the GPC elution volumes are very sensitive not only to the type of column used but also to the column's history. Because of these differences, direct comparisons of the elution volumes from the different laboratories cannot be made even though the behavior of the SBM molecular weight distributions and the trends observed as a function of arm molecular weight are valid.

Branching Characteristics. Branching is commonly characterized by shrinking factors. The following shrinking factors are commonly in use[1-3,23]

$$g = R_{g,b}^2/R_{g,lin}^2 \tag{6}$$

$$h = R_{h,b}/R_{h,lin} = D_{lin}/D_b \tag{7}$$

$$g' = [\eta]_b/[\eta]_{lin} \tag{8}$$

$$g_{A_2} = A_{2,b}/A_{2,lin} \tag{9}$$

where all ratios have to be taken at the same molecular weight, and the subscripts "b" and "lin" refer to branched and linear polymers, respectively, of the same molecular weight. These shrinking factors are clearly defined for regularly branched structures, which by definition are monodisperse. Most branched materials, however, are polydisperse, and, in such cases, the shrinking factors have some ambiguities. In the following, we define the shrinking factors as ratios at the same *weight-average molecular weight*, if not otherwise indicated.

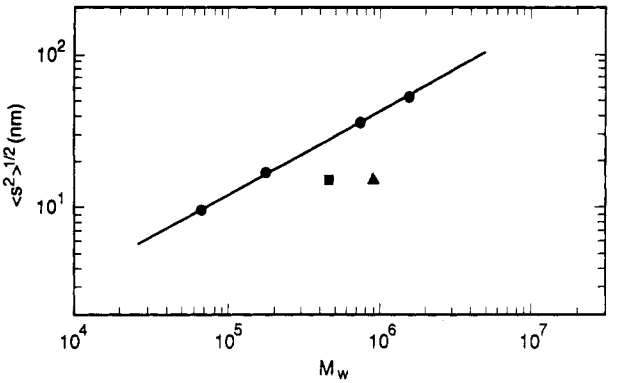

Figure 6. Logarithmic plot of $\langle S^2 \rangle_z^{1/2}$ as a function of M_w for a series of linear PMMA (–●–) and star microgels (■, ▲) in THF. The filled symbols refer to the fractionated samples.

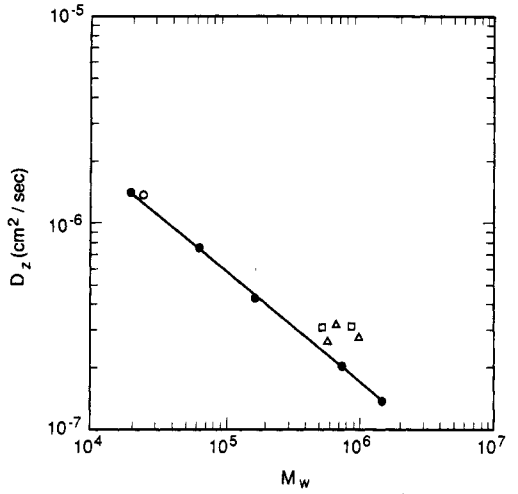

Figure 7. Plot of D_z versus M_w for linear PMMA and the star-branched microgels: linear PMMA (●); L10 (○); S10f and S20f (□); S21a, S21b, and S21c (△).

In addition to the above shrinking factors, a parameter[24] ρ is used, which is the ratio of the radius of gyration, R_g, and the hydrodynamic radius, R_h.

$$\rho = R_g/R_h \tag{10}$$

For the determination of the shrinking factors, the conformational and thermodynamic properties of the corresponding linear chain have to be known. To this end, four GTP-polymerized PMMA samples from the Röhm Co., Darmstadt, were measured in THF. In addition, one sample (L10) was obtained by a preparative fractionation of the product S10; the lowest molecular weight linear PMMA (sample PL1) was prepared by the Freiburg group by GTP. These six samples have a fairly low polydispersity and cover a range of molecular weight from M_w = 20 000 to $M_w = 1.47 \times 10^6$.

The results for $\langle S^2 \rangle_z$, D_z, $[\eta]$, and A_2 of these linear chains are shown in Figures 6–9, together with data of the star-branched microgels. The molecular weight dependences of these parameters for the linear PMMA chain in THF are

$$R_{g,lin} = 2.18 \times 10^{-2} M_w^{0.54} \tag{11}$$

$$D_{z,lin} = 3.87 \times 10^{-4} M_w^{-0.54} \tag{12}$$

$$[\eta]_{lin} = 1.70 \times 10^{-2} M_w^{0.66} \tag{13}$$

$$A_2 = 7.20 \times 10^{-3} M_w^{-0.21} \tag{14}$$

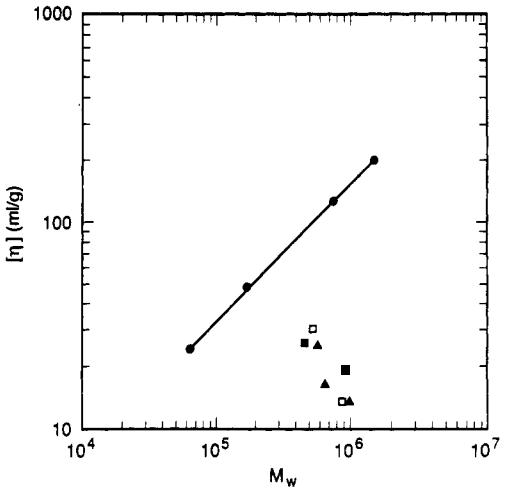

Figure 8. Plot of $[\eta]$ versus M_w for linear PMMA and star-branched microgels: linear PMMA (●); S10f and S20f (■); S10 and S20 (□); S21a, S21b, and S21c (▲).

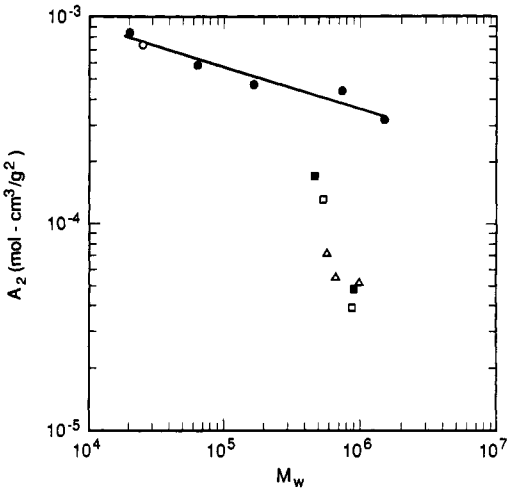

Figure 9. A_2 as a function of M_w for linear PMMA and star microgels: linear PMMA (●), L10 (○); S10f and S20f (■); S10 and S20 (□); S21a, S21b, and S21c (△).

which show the usual scaling behavior of chains in a marginal solvent[25] with $\nu = 0.545 \pm 0.005$ in the equations $R_g \sim M^{\nu}$, $D \sim M^{-\nu}$, and $[\eta] \sim M^{3\nu-1}$. The exponent in A_2 is, with $a_{A_2} = -0.21$, smaller in magnitude than the value of $3\nu - 2 = -0.36$.

The deviation of a_2 from $3\nu - 2$ results from the marginal solution behavior[26] that can be suitably described by the interpenetration function $\psi(z)$ in the relationship for A_2

$$A_2 = 4\pi^{3/2} N_A (R_g^3/M^2) \psi(z) \tag{15}$$

Here, $z \sim \beta N^{1/2}$ is the usual thermodynamic interaction parameter with β the segment excluded volume and N the number of segments per macromolecule. A small value of ψ^* indicates deep interpenetration whereas the high value of $\psi^*_{sphere} = 1.61$ for hard spheres denotes no interpenetration at all. For the PMMA samples in THF, z remains fairly small since THF is a marginal solvent and $\psi(z)$ has not yet reached its final constant value. $\psi(z)$ still shows an increase with growing molecular weight and thus reduces the negative exponent in the term R_g^3/M^2 from –0.36 to –0.21.

One notices the expected shrinking from the data of $R_{g,b}$, $[\eta]_b$, and $A_{2,b}$ and the corresponding increase of $D_{z,b}$; the deviations from linear chain behavior become more pronounced for the star-branched microgels with the larger number of arms. The results of shrinking factors are collected in Table IV.

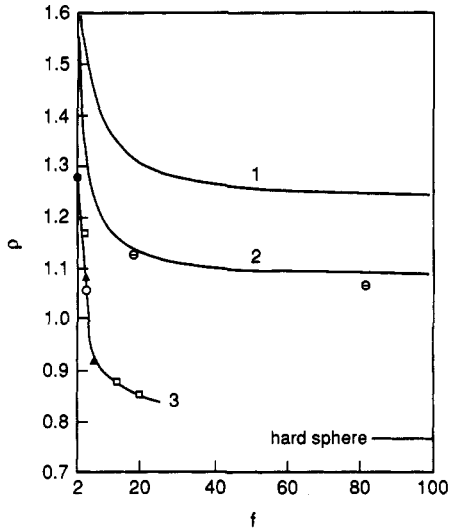

Figure 10. ρ parameter for regular star macromolecules and for star-branched microgel samples S10f and S20f (○). Curve 1: theory for polydisperse arms ($M_w/M_n = 2$). Curve 2: theory for monodisperse arms.[24] Curve 3: experiment in cyclohexane: 3-, 12-, and 18-armed PS stars[31] (□); 4- and 6-armed PS stars[40] (▲); cyclic PS chains[39] (○); linear PS chains[41] (●).

The values of the ρ-parameter are plotted in Figure 10 as a function of the number of arms together with the theoretical relationship for regular star molecules (monodisperse as well as polydisperse) and data for regular star polymers.[24] The experimental values of ρ for monodisperse regular stars decrease with an increasing number of arms, approaching the hard-sphere value more rapidly than theory for monodisperse regular stars. In contrast, for SBM's, ρ appears to be well represented by theory for monodisperse regular stars. We believe that this correlation is fortuitous and that the larger ρ values for the star-branched microgels reflect their polydispersity ($M_w/M_n \sim 1.8$). This is suggested by the increase in ρ predicted by theory for polydisperse regular stars as shown in Figure 10.

Discussion

We first discuss the effects of branching on the dimensions of the particles and on A_2 and then turn to a more detailed consideration of the molecular weight distribution.

Shrinking Factors. As already mentioned, the experimental shrinking factors g and h are considerably larger than those for the corresponding regular stars. This is to some extent caused by the polydispersity.[27] As is shown in Table IV after correction of $\langle S^2\rangle_z$ to $\langle S^2\rangle_w$, the $g_w = \langle S^2\rangle_{w,b}/\langle S^2\rangle_{w,lin}$ is reduced significantly for S10f and S20f. However, g_w is still larger than predicted for regular stars. For the h factors, the polydispersity correction has little influence and the experimental data remain much larger than predicted. This behavior may be understood as follows. The large number of chains attached to a nucleus of rather small extension is crowded. This results in a stretching out of the arms, which is larger close to the star center than at the periphery.[29-31] This position-dependent stretching out partly compensates the shrinking effect due to branching. It is of interest that this overcrowding of segments has a stronger effect on the hydrodynamic radius. Similar behavior has been found already with the regular star molecules[31] if the number of arms is larger than $f = 8$. The lower values of the ρ-parameters are then the necessary consequence of this observation that R_h is more strongly effected by the overcrowding than R_g.

For the g' factor, the accurate values are not yet known from theory. Zimm and Kilb[2] suggested that for a large number of arms the behavior of $g' \sim g^{1/2}$. Our results suggest a direct proportionality and agree satisfactorily with the experimental data of other laboratories[23,32-36] if g_w is used. This is shown in Figure 11 where g' is plotted against g. The point for $f = 80$ (sample S10f) appears to deviate from the line that would be expected from the experimental data. However, the g' parameter can in real cases never become smaller than a certain value that corresponds to the intrinsic viscosity of a densely packed homogeneous sphere, i.e., $[\eta] = 2.5v_2$, where v_2 is the partial specific volume of the polymer. Thus, the curve in Figure 11 must eventually level off for very large arm numbers. The intrinsic viscosity of the S10f sample is only 7 times the homogeneous sphere value, and an influence of such dense packing may be already important. No corrections for polydispersity have been applied to $[\eta]_b$ and thus to g'. The effect of polydispersity is low here[38] since $[\eta] \sim V_{h,n}/M_n$ is a ratio of two number averages, which depends only weakly on M_w/M_n.

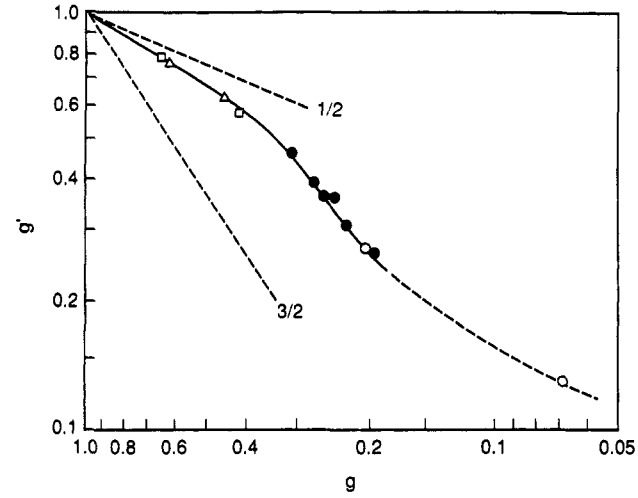

Figure 11. Dependence of g' on g according to experiments: star-branched microgels (○); regular star molecules (□), (△), and (●).

The decrease of A_2 as a consequence of branching follows from theory[4,26] to be

$$g_{A_2} = (R_{g,b}^3/R_{g,lin}^3)(\psi_b(z)/\psi_{lin}(z)) = g^{3/2}\psi_b(z)/\psi_{lin}(z) \quad (16)$$

For large z (large excluded volume, good solvent condition), the interpenetration functions attain a constant value ψ^*. The function ψ^*_b was found in theory[37] and experiment[23,35] to increase with branching but never should become larger than the corresponding value for a hard sphere,[35] $\psi^*_{sphere} = 1.61$. Figure 12 shows the experimentally observed values from regular star molecules and the present SBM's where the polydispersity of the SBM's has been taken into account. The data for the SBM's lie higher than those for the corresponding regular stars, and for the highly branched star microgel, the value of a hard sphere is already reached. Thus, g_{A_2} should be larger than $g^{3/2}$, which is indeed observed. The continuous line in Figure 12 represents the prediction of the renormalization theory,[37] which shows agreement with experiment only up to $f = 6$.

GPC. Gel permeation chromatography data are usually evaluated on the basis of the following universal calibration relationship[11]

$$\ln V_h = V_0 - mV_e \equiv V'_e \quad (17)$$

where $V_h = [\eta]M$ is the effective hydrodynamic volume of the polymer, V_0 is the exclusion volume below which no

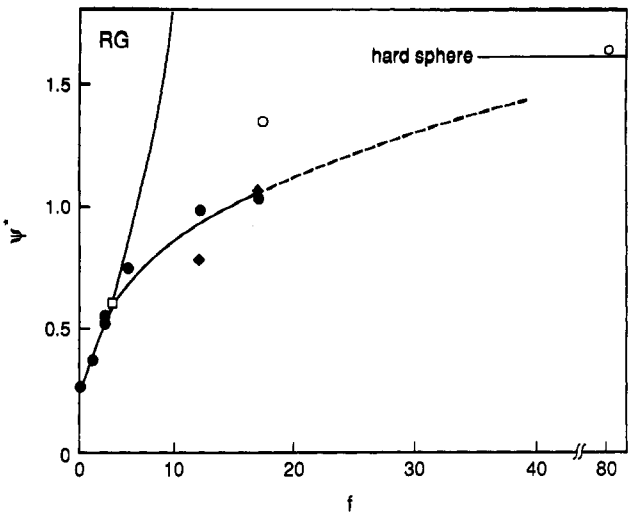

Figure 12. Maximum interpenetration function ψ^* as a function of the arm number f; (○) star microgels; (●) regular star molecules; (□) cyclic chain,[40] which corresponds to a star of $f = 4.5$. The continuous line represents the prediction by the renormalization group theory.

separation occurs, V_e is the elution volume, and m is a constant that describes the efficiency of the separation.

Assuming validity of the Fox–Flory relationship[5] also for branched molecules, one can write

$$[\eta]_{lin} = \phi'_{lin}(V_h/M)_{lin}$$

and

$$[\eta]_b = \phi'_b(V_h/M)_b \tag{18}$$

Dividing the two equations, under the assumption that the molecular weights of the branched and the linear sample are the same, one has

$$[\eta]_b/[\eta]_{lin} = g' = (\phi'_b/\phi'_{lin})(V_{h,b}/V_{h,lin}) \tag{19}$$

and with eq 17

$$\ln (V_{h,b}/V_{h,lin}) = V'_{e,b} - V'_{e,lin} \equiv \Delta V'_e \tag{20}$$

Defining $h' = \exp(\Delta V'_e)$, one finally finds

$$h' = g'(\phi'_{lin}/\phi'_b) \tag{21}$$

Parts a and b of Figure 13 are plots of h' as a function of the number of arms per microgel for the two different sets of SBM's. Within experimental error, the star-branched microgels studied at the same laboratory show the same dependence on the number of arms per nucleus. The data from the different laboratories, however, exhibit a different dependence on f. In spite of this discrepancy, the results from each laboratory independently suggest that not only g' but also the ratio ϕ'_{lin}/ϕ_b are functions solely of the number of arms and do not depend on the arm length. The arm length independence of ϕ'_{lin}/ϕ_b indicates a constant draining. As indicated in our discussion of g_w, crowding and stretching of the arms occurs, suggesting non-Gaussian statistics. Consequently, in contrast to Gaussian chain behavior, one might expect that the ratio of hydrodynamic volumes is *not* independent of the arm molecular weight. That we find this ratio as well as the draining to be independent of arm molecular weight is therefore surprising.

Acknowledgment. M.S.W. thanks B. L. Neff for helpful discussions and H. H. Stutting of LDC/Milton Roy Co. for performing the GPC–LALLS measurements on three of the star-branched microgels. P.L. and W.B. thank the Rohm Co., Darmstadt, for supplying them with four monodisperse linear PMMA samples.

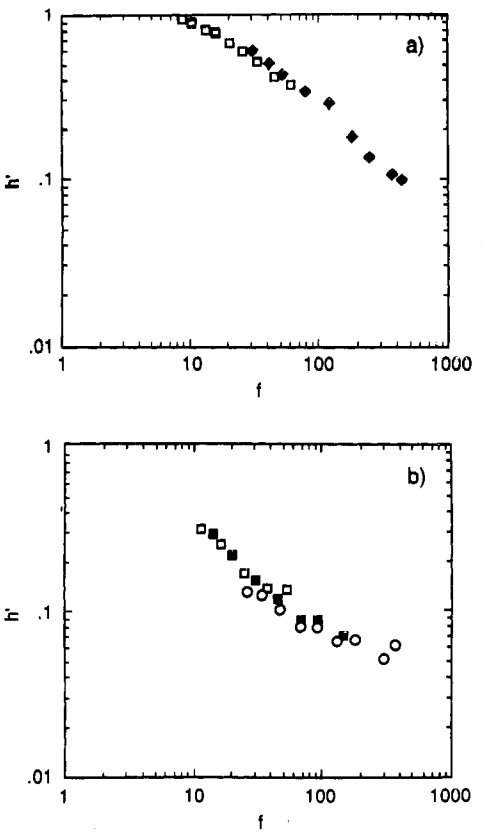

Figure 13. Plot of $h' = \exp(\Delta V'_e)$ (eq 16) against the number of arms: (a) samples S10f (◆) and S20f (□); (b) samples S21a (○), S21b (■), and S21c (□).

References and Notes

(1) Zimm, B. H.; Stockmayer, W. H. *J. Chem. Phys.* **1949**, *17*, 1301.
(2) Zimm, B. H.; Kilb, R. W. *J. Polym. Sci., Polym. Phys. Ed.* **1959**, *37*, 19.
(3) Stockmayer, W. H.; Fixman, M. *Ann. N.Y. Acad. Sci.* **1953**, *57*, 334.
(4) Casassa, E. F. *J. Phys. Chem.* **1962**, *37*, 2176.
(5) Flory, P. J. *Principles of Polymer Chemistry*; Cornell University Press: Ithaca, NY, 1953.
(6) Kajiwara, K.; Burchard, W.; Gordon, M. *Br. Polym. J.* **1970**, *2*, 110.
(7) Kajiwara, K. *Polymer* **1971**, *12*, 57.
(8) Burchard, W. *Adv. Polym. Sci.* **1983**, *48*, 1.
(9) (a) Webster, O. W.; Hertler, W. R.; Sogah, D. Y.; Farnham, W. B.; Rajan Babu, T. V. *J. Am. Chem. Soc.* **1983**, *105*, 5706. (b) Webster, O. W.; Hertler, W. R.; Sogah, D. Y.; Franham, W. B.; Rajan Babu, T. V. *J. Macromol. Sci., Chem.* **1984**, *A21*, 943. (c) Simms, J. A.; Spinelli, H. J. *J. Coat. Technol.* **1987**, *59*, 125.
(10) Eschwey, H.; Burchard, W. *Polymer* **1975**, *16*, 180.
(11) Grubisic, Z.; Rempp, P.; Benoit, H. *J. Polym. Sci.* **1967**, *B5*, 753.
(12) Lang, P.; Burchard, W. *Makromol. Chem., Rapid Commun.* **1987**, *8*, 451.
(13) Müller, M. A.; Stickler, M.; Burchard, W. *Makromol. Chem., Rapid Commun.* **1986**, *7*, 575.
(14) Bantle, S.; Schmidt, M.; Burchard, W. *Macromolecules* **1980**, *13*, 580.
(15) Danliker, W. B.; Krautt, J. *J. Am. Chem. Soc.* **1956**, *78*, 2380.
(16) Bodmann, O. *Makromol. Chem.* **1969**, *122*, 196.
(17) Friedman, H. L. *A Course in Statistical Mechanics*; Prentice Hall: Englewood Cliffs, NJ, 1985.
(18) Burchard, W., unpublished data.
(19) Berry, G. C. *J. Chem. Phys.* **1966**, *44*, 4550.
(20) Koppel, D. E. *J. Chem. Phys.* **1972**, *57*, 4814.
(21) Berne, B.; Pecora, R. *Dynamic Light Scattering*; Wiley: New York, 1976.
(22) Pusey, P. N.; Koppel, D. E.; Schaefer, D. W.; Comerini-Otero, R. D.; Koenig, S. H. *Biochemistry* **1974**, *13*, 952.
(23) Bywater, S. *Adv. Polym. Sci.* **1979**, *30*, 90.

(24) Burchard, W.; Schmidt, M.; Stockmayer, W. H. *Macromolecules* **1980**, *13*, 1265.
(25) de Gennes, P.-G. *Scaling Concepts in Polymer Physics*; Cornell University Press: Ithaca, NY, 1979.
(26) Yamakawa, H. *Modern Theory of Polymer Solutions*; Harper & Row: New York, 1971.
(27) Assuming a Schulz–Zimm type distribution, one has[28] $\langle S^2\rangle_z/\langle S^2\rangle_w = (z+1+2\nu)/(z+1)$ with $1/z = M_w/M_n - 1$. The data of M_w/M_n as given in Table II were used.
(28) Zimm, B. H. *J. Chem. Phys.* **1948**, *16*, 1093.
(29) Daoud, M.; Cotton, P. J. *J. Phys.* **1982**, *43*, 531.
(30) Birshtein, T. M.; Zhulina, E. B. *Polymer* **1984**, *25*, 1453.
(31) Huber, K.; Burchard, W.; Fetters, L. J. *Macromolecules* **1984**, *17*, 541.
(32) Roovers, J. E. L.; Bywater, S. *Macromolecules* **1972**, *5*, 384.
(33) Roovers, J. E. L.; Bywater, S. *Macromolecules* **1974**, *7*, 443.
(34) Meunier, J.-G. *Makromol. Chem.* **1971**, *147*, 191.
(35) Roovers, J. E. L.; Hajichristidis, N.; Fetters, L. J. *Macromolecules* **1983**, *16*, 214.
(36) Bohdanecky, M. *Macromolecules* **1977**, *10*, 971.
(37) Douglas, J. F.; Freed, K. F. *Macromolecules* **1984**, *17*, 1854.
(38) Marriman, J.; Hermans, J. J. *J. Phys. Chem.* **1961**, *65*, 385.
(39) Roovers, J. E. L. *J. Polym. Sci., Polym. Phys. Ed.* **1985**, *23*, 1117.
(40) Roover, J.; Toporowski, P. M. *J. Polym. Sci., Polym. Phys. Ed.* **1980**, *18*, 1917.
(41) Schmidt, M.; Burchard, W. *Macromolecules* **1981**, *14*, 210.

Registry No. PMMA/EGDMA, 25777-71-3.